

Ultrasound-activated Agents Comprised of 5FU-bearing Nanoparticles Bonded to Microbubbles Inhibit Solid Tumor Growth and Improve Survival

Caitlin W Burke¹, Eben Alexander IV¹, Kelsie Timbie¹, Alexander L Kilbanov^{1,2} and Richard J Price^{1,3,4}

¹Department of Biomedical Engineering, University of Virginia, Charlottesville, Virginia, USA; ²The Cardiovascular Division, University of Virginia, Charlottesville, Virginia, USA; ³Department of Radiology, University of Virginia, Charlottesville, Virginia, USA; ⁴Department of Radiation Oncology, University of Virginia, Charlottesville, Virginia, USA

Nanoparticle (NP) drug delivery vehicles may eventually offer improved tumor treatments; however, NP delivery from the bloodstream to tumors can be hindered by poor convective and/or diffusive transport. We tested whether poly(lactic-co-glycolic acid) NP delivery can be improved by covalently linking them to ultrasound (US)-activated microbubbles in a “composite-agent” formulation and whether drug 5-fluorouracil (5FU)-loaded NPs delivered in this fashion inhibit the growth of tumors that are typically not responsive to intravenously administered 5FU. After intravenous composite-agent injection, C6 gliomas implanted on Rag-1^{-/-} mice were exposed to pulsed 1 MHz US, resulting in the delivery of 16% of the initial NP dose per gram tissue. This represented a five- to 57-fold increase in NP delivery when compared to multiple control groups. 5FU-bearing NP delivery from the composite-agent formulation resulted in a 67% reduction in tumor volume at 7 days after treatment, and animal survival increased significantly when compared to intravenous soluble 5FU administration. We conclude that NP delivery from US-activated composite agents may improve tumor treatment by offering a combination of better targeting, enhanced payload delivery, and controlled local drug release.

Received 1 August 2013; accepted 17 October 2013; advance online publication 10 December 2013. doi:10.1038/mt.2013.259

INTRODUCTION

Achieving uniform drug delivery throughout solid tumors remains a difficult problem.¹ Pharmacological barriers include high molecular weight, low solubility, short half-life, and/or systemic toxicity, while physiological barriers include limited convective transport at the core of the tumor due to high interstitial pressures (8–30 mm Hg)² as well as size-dependent extravascular and interstitial diffusion limitations.^{3–5} Encapsulating chemotherapeutic agents in nanocarriers (*i.e.*, nanoparticles (NP) and liposomes) enables limitations associated with solubility, systemic toxicity, and/or bioavailability to be overcome. Degradable polymers, such as poly(lactic-co-glycolic acid) (PLGA), have the potential to prolong drug release.⁶ Some systemically administered drug delivery

vehicles preferentially accumulate in growing tumors that exhibit a leaky vasculature and the enhanced permeability and retention effect.^{7–9} However, high interstitial pressures often are present,^{2,3} which can limit the extravasation of larger convection-dependent nanocarriers.² Diffusive transport dominates in the tumor core; however, diffusion is increasingly ineffective as particle size, charge and distance in the tissue from the nearest blood vessel increase.^{4,5} Taken together, poor convective and diffusive transport may result in heterogeneous nanocarrier accumulation, which may contribute to reduced responsiveness to chemotherapy.

The activation of contrast agent microbubbles (MBs) with ultrasound (US) is emerging as a powerful strategy for overcoming physiological barriers associated with drug and gene delivery.^{10–14} It is generally thought that contrast agent MB expansion and collapse in an acoustic field facilitates the delivery of intravascularly administered drugs/genes to tissue by permeabilizing cellular membranes¹¹ and/or the microvasculature,^{10,12} with permeabilization responses being dependent on acoustic settings, MB dimensions, and MB concentration. Ultrasonic activation of MBs coadministered with nanocarriers has resulted in increased nanocarrier delivery to a variety of tissues, including tumors.^{14–19} Furthermore, as demonstrated by our group¹⁴ and others,^{20–23} improvements in nanocarrier delivery may be made by conjugating them to MBs. We recently demonstrated that covalently linking PLGA NPs to MBs to form so-called MB-NP composite agents (MNCAs) before intravenous (*i.v.*) injection can improve their delivery to ischemic skeletal muscle.¹⁴ Here, MNCAs were targeted to subcutaneous C6 gliomas. Our first objective was to enhance NP delivery to these tumors through the use of US-activated MNCAs. Our second objective was to determine the therapeutic efficacy of the approach when delivering 5-fluorouracil (5FU)-bearing PLGA NPs. Our results indicate that ultrasonic activation of MBs bound to 5FU-bearing NPs increases NP delivery to tumor, producing dose-dependent tumor growth inhibition and prolonged survival.

RESULTS

Characterization of MB-NP composite agents

Mean initial MB diameter, as determined with a Coulter Counter (Multisizer-IIe; Beckman Coulter, Brea, CA), was

Correspondence: Richard J Price, Department of Biomedical Engineering, University of Virginia, Box 800759, Health System, Charlottesville, Virginia 22908, USA. E-mail: rprice@virginia.edu

$2.19 \pm 1.36 \mu\text{m}$. Fluorochrome-labeled tracer NPs, created by binding VivoTag680 (VT680) to BSA PLGA NPs, exhibited a mean diameter of $154.9 \pm 79.7 \text{ nm}$ (Figure 1a), as determined with a submicron-particle analyzer (Multisizer IIe; Beckman Coulter). Zetasizer (Zetasizer 3000; Malvern Instruments, Worcestershire, UK) analysis revealed a zeta potential of $-43.3 \pm 3.9 \text{ mV}$. PLGA NPs exhibited an average of 920 VT680 fluorochromes per NP as determined spectrophotometrically. Covalently coupling VT680 NPs to MBs resulted in an average of 518 ± 236 NPs per MB, as determined by UV-visible spectroscopy (Ultrospec 3000; Pharmacia Biotech, Piscataway, NJ). The mean diameter of VT680-MNCAs was determined to be $1.72 \pm 1.28 \mu\text{m}$, indicating that some gas had diffused from the MB cores as they were being manipulated to generate the MNCAs. Flow cytometry imaging performed on an

ImageStream device (Amnis, Seattle, WA) revealed a mean MB intensity of 215.6 for the MNCA group, 31.8 for MBs incubated with NPs, and 24.0 for MBs alone (Figure 1b). Results indicate that there was essentially no nonspecific association of NPs with MBs in the coinjection group. For 5FU-loaded NPs, submicron-particle analysis (Multisizer IIe; Beckman Coulter) revealed a mean NP diameter of $126.9 \pm 64.3 \text{ nm}$ (Figure 1c), while Zetasizer (Zetasizer 3000; Malvern Instruments) measurements yielded a zeta potential of $-40.1 \pm 3.6 \text{ mV}$. *In vitro* loading and release studies were performed on a nanosuspension containing 5FU-NPs in phosphate-buffered saline. Encapsulation efficiency, defined as the ratio of amount of drug encapsulated to that of the drug used in the NP preparation, was 8%. PLGA NPs demonstrated controlled release of 5FU over a 2-week period (Figure 1d), reaching 91% total drug release at day 15.

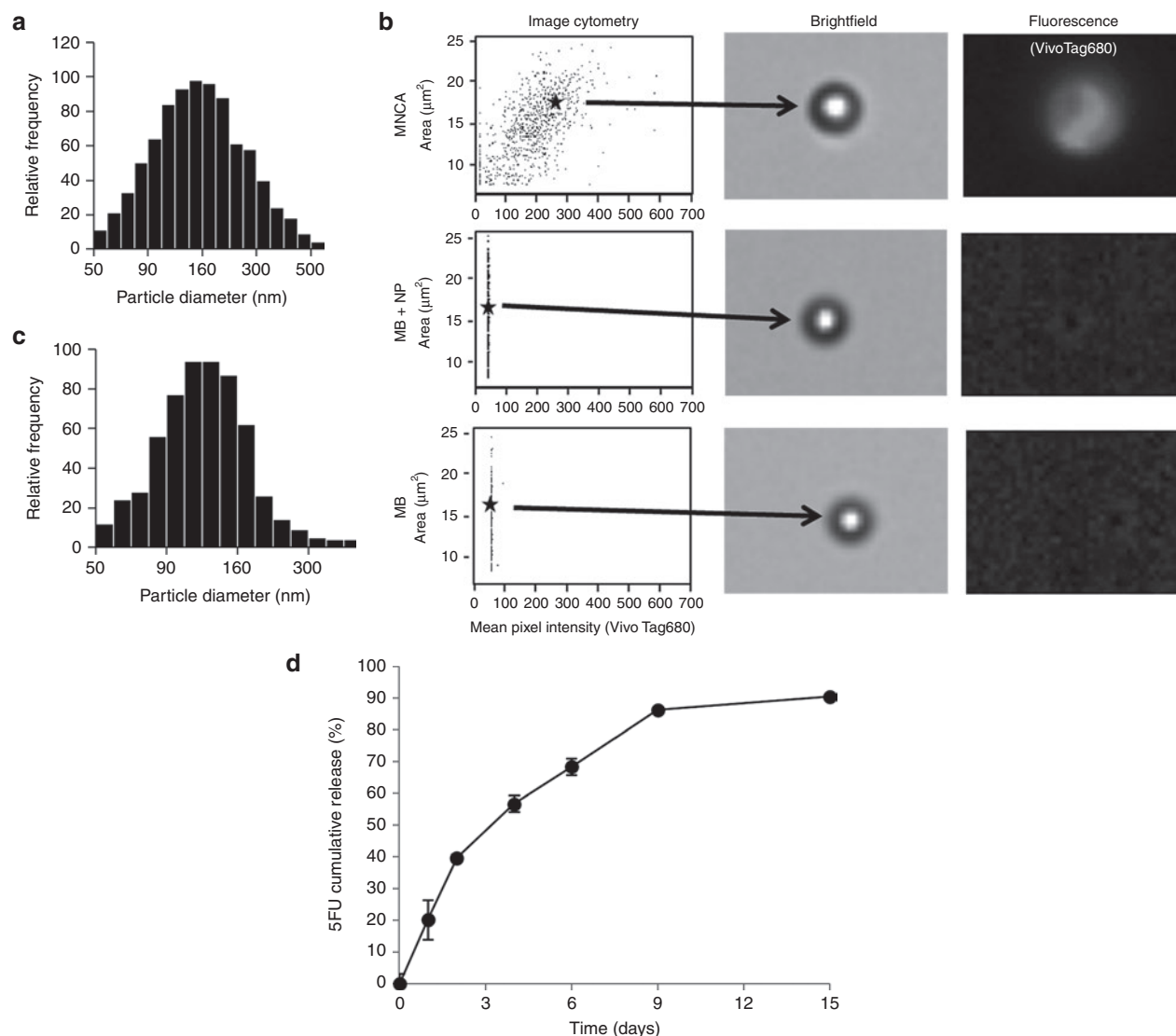


Figure 1 Characterization of microbubble (MB)-nanoparticle (NP) composite agents (MNCAs). **(a)** Number weighted NiComp bovine serum albumin (BSA) bearing nanoparticle size distribution. **(b)** Image Stream scatterplot data with brightfield and fluorescence images corresponding to selected data points for the MNCA, MB+NP, and MB formulations. Mean fluorescence pixel intensities were 215.6, 31.8, and 24.0 for the MNCA, MB+NP, and MB formulations, respectively. Data illustrate the successful linking of NPs to MBs in the MNCA formulation, as well as lack of adhesion between NPs and MBs in the coinjection group. **(c)** Number weighted NiComp 5-Fluorouracil (5FU) bearing NP size distribution. **(d)** Line graph showing cumulative 5FU release from PLGA NPs ($n = 5$ replicates). Error bars are means \pm SEM, with some bars hidden by data points.

NP delivery to tumors is dependent on both US and MBs when using an intravenous Coinjection strategy

Fluorescence molecular tomography (FMT) was used to analyze NP delivery at 0, 1, 2, and 4 hours after applying US to one of two bilaterally implanted C6 glioma tumors (Figure 2a). Later time points were not considered because albumin-shelled MBs are cleared on the order of minutes,²⁴ while PLGA NPs in this diameter range are almost entirely cleared from the circulation within 1 hour.²⁵ The subcutaneous C6 glioma model was chosen as a representative example of a well-vascularized²⁶ solid tumor. For both the MNCA (Figure 2a; top row) and MB+NP coinjection (Figure 2a; middle row) groups, fluorescence intensity was clearly greater on the US-treated side when compared to the contralateral “no US” side, with the MNCA+US treated tumors also showing greater NP delivery than the MB+NP+US treated tumors. Applying US to intravenously injected NPs without MBs present yielded little increase in fluorescence intensity (Figure 2a; bottom row).

FMT scans were quantitatively analyzed to determine the % initial dose (ID) per gram of tumor mass at 0, 1, 2, and 4 hours after treatment (Figure 2b). The effect of US application on NP delivery within the coinjection group is illustrated by comparing the MB+NP+US group to the MB+NP group. As expected based on previous studies,^{15–17} US application caused a significant increase in NP delivery, with pairwise comparisons revealing a 4.1-fold increase in NP delivery at 4 hours. Meanwhile, the effect of MBs on NP delivery is shown by comparing the MB+NP+US group to the NP+US group. MBs had a significant effect on NP delivery overall, with pairwise comparisons revealing 3.7- and 8.2-fold increases in NP delivery at 1 and 4 hours, respectively. Applying US to systemically administered NPs without MBs present did not significantly affect NP delivery. Figure 3 shows representative confocal microscopy images of US-treated tumor tissue 4 hours after the i.v. injection of MNCA (Figure 3; top row), MB+NPs (Figure 3; middle row), or NPs (Figure 3; bottom row). NPs,

which were labeled with a far-red fluorophore (VT680) in these studies, have been false-colored to red, while capillaries appear green. In general agreement with the FMT data in Figure 2, overall NP delivery appeared significantly greater for the MB+NP+US group when compared to the MB+NP (not shown in Figure 3) and NP+US groups. For the MB+NP+US group, many NPs were colocalized with BS-I lectin, indicating endothelial delivery. The remaining NPs were present in the extravascular space, indicating some interstitial delivery had also occurred. In contrast, US application to NPs in the absence of MBs (Figure 3; bottom row) yielded virtually no detectable NP delivery.

Covalently coupling NPs to MBs before intravenous injection enhances their US-targeted delivery to tumors

Within the MNCA group, US application elicited statistically significant 6.2-, 8.3-, and 6.6-fold increases in NP delivery at 0, 1, and 4 hours after MNCA treatment, respectively, when compared to contralateral “no US” controls (Figure 2). NPs were colocalized with BS-I lectin and also present in the extravascular space (Figure 3; top row).

Total injected MB and NP concentrations were identical for both the MB+NP and MNCA groups. In addition, the US application protocol was uniform throughout the study. Therefore, we were able to test whether coupling MBs to NPs in the MNCA formulation results in improved NP delivery to tumor tissue by comparing the MNCA+US and MB+NP+US groups. At 0, 1, and 4 hours after US application, NP delivery was 5.6-, 4.9-, and 2.5-fold higher for the MNCA+US group when compared to the MB+NP+US group (Figure 2b). Confocal observations of tumors from the MNCA+US group confirmed a substantial increase in NP delivery when compared to the MB+NP+US coinjection group (Figure 3). Four hours after treatment with MNCA, the liver, kidney, spleen, lungs, heart, US-treated tumor, and contralateral “no US” control tumor were excised, and FMT was used to

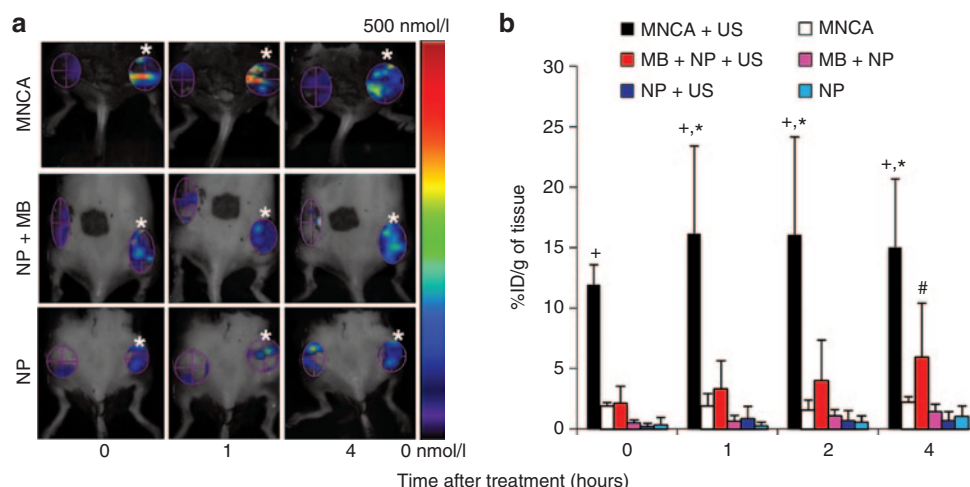


Figure 2 Fluorescence-molecular tomography scans showing, and bar graphs quantifying, nanoparticle (NP) delivery to tumor at various time points after treatment. (a) Top row: composite agent (MNCA) injection. Middle row: coinjection of microbubbles (MBs) and NPs. Bottom row: NP injection without microbubbles. Ultrasound (US)-treated tumors are denoted with white asterisks. Enhanced fluorescence intensity is evident with US application for the MNCA and MB+NP groups when compared to contralateral tumors that did not receive US. (b) Bar graph of fluorochrome concentration (% initial dose (ID) per gram of tissue) as a function of time. Bars are means \pm SD. *Significantly different than MNCA at $P < 0.05$. #Significantly different than MB+NP+US at $P < 0.05$. *Significantly different than MB+NP at $P < 0.05$. All groups, $n = 4$.

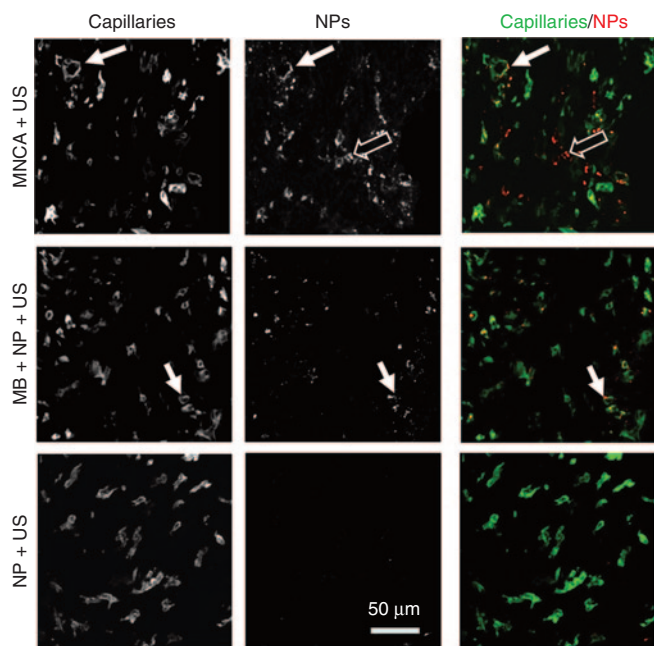


Figure 3 Confocal images of cross-sectioned tumor at 4 hours after ultrasound application. Top row: Composite agent (MNCA) injection. Middle row: Coinjection of microbubbles (MBs) and nanoparticles (NPs). Bottom row: NP injection without microbubbles. Left column: Capillaries labeled with BS-I lectin. Middle column: VT680-conjugated NPs that have been delivered to tissue. Right column: merge images showing delivered NPs (red) with respect to capillaries (green). Filled arrows denote colocalization of NPs and capillary endothelium. Open arrows denote regions where NPs have been delivered beyond the endothelium to the interstitial space.

analyze NP accumulation. Quantitative results from FMT organ scans are shown in [Figure 4](#).

Tumor growth is inhibited by 5FU-bearing NP delivery with US and MBs

Changes in tumor volume were quantified after treatment with 5FU-bearing MNCAs+US, BSA-bearing MNCAs+US, 5FU-bearing MNCAs without US, and intravenously administered soluble 5FU ([Figure 5a](#)). Significant tumor growth inhibition was observed following US activation of 5FU-bearing MNCAs when compared to all other groups. Specifically, the US-targeted delivery of 5FU-NPs from the MNCA formulation resulted in an ~50% reduction in tumor volume at 7 days after treatment when compared to controls in which US was not applied, as well as to controls in which “blank” BSA NPs or soluble 5FU were delivered ([Figure 5a](#)).

Because the total dosage of 5FU used in the studies for [Figure 5a](#) was significantly lower than may be used clinically, we next tested whether increasing the dosage of 5FU via an increase in MNCA concentration could result in improved tumor growth inhibition. Before doing this, we needed to ensure that total MNCA dosage has no significant influence on NP delivery (*i.e.*, %ID/g of tumor tissue). To this end, FMT was used to quantify NP delivery at 0, 1, and 4 hours after *i.v.* administration of MNCAs at “high” (10^7 MNCAs/g) and “standard” (10^5 MNCAs/g) doses and the application of US. As shown in [Figure 5b](#), no statistically significant differences in %ID/g of tumor tissue were observed.

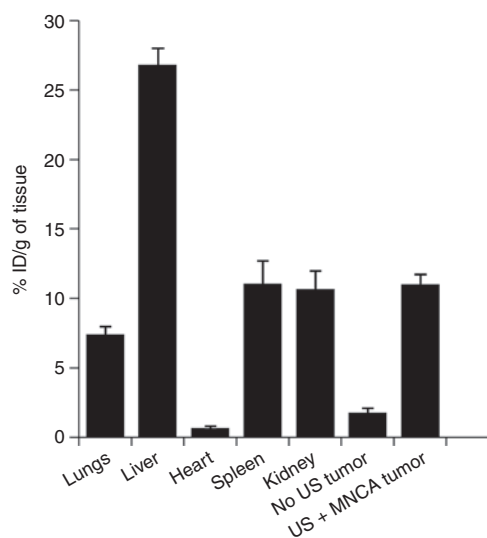


Figure 4 Nanoparticle biodistribution 4 hours after MNCA+US treatment. Bar graph of fluorochrome concentration (% initial dose (ID) per gram of tissue) in ultrasound (US)-treated tumor and “off-target” tissues and organs as determined by fluorescence molecular tomography. Bars are means + SD.

Thus, tumors treated with a “high” dose of MNCAs received an approximately proportional increase in 5FU when compared to the “standard” dose group.

The dose-dependent effects of treatment were then assessed through the quantification of tumor volume after treatment with 5FU-bearing MNCAs and US at “standard” and “high” doses, as well as treatment with 5FU-bearing MNCAs without US activation at “standard” and “high” doses ([Figure 5c](#)). US activation of “high” dose 5FU-MNCAs elicited statistically significant 23 and 36% reductions in tumor volume at 6 and 7 days after treatment, respectively, when compared to treatment with US-delivered “standard” dose 5FU-MNCAs, indicating that enhanced anti-tumor efficacy may be achieved by increasing injected MNCA concentration.

Finally, we tested whether the delivery of 5FU-bearing NPs via the US activation of MNCAs could enhance the survival of mice with single C6 gliomas. Mice receiving *i.v.* administered soluble 5FU served as the control group in these studies. Survival data according to the Kaplan–Meier analysis²⁸ are presented in [Figure 5d](#). Here, the survival time for mice receiving “high” dose MNCA treatment was significantly greater than for mice treated with *i.v.* soluble 5FU ($P = 0.041$).

DISCUSSION

We^{14–17} and others^{18,19} have demonstrated that the application of US after the intravascular coinjection of NPs and MBs results in targeted NP delivery. Furthermore, there is compelling evidence that physically linking NPs to MBs may further improve NP delivery upon activation with US.^{14,20–23} Here, we applied these concepts to an *in vivo* solid tumor model and report two major findings. First, we determined that covalently linking NPs to MBs increases NP delivery to US-targeted subcutaneous solid tumors when compared to the intravascular coinjection of NPs and MBs ([Figures 2 and 3](#)). Second, using this same US-targeted approach,

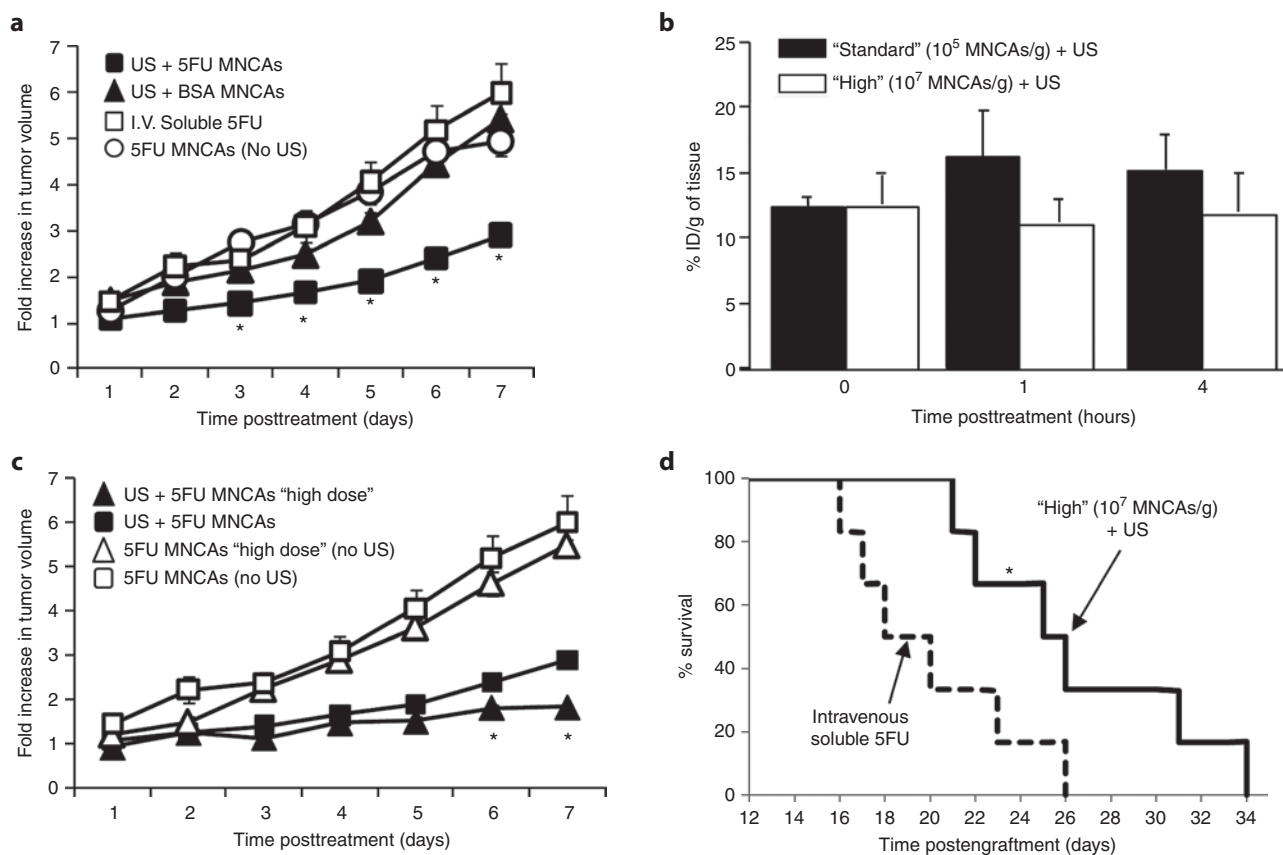


Figure 5 Ultrasound (US) activation of 5FU-bearing MNCAs inhibits growth of subcutaneous C6 gliomas in vivo. **(a)** Fold change in tumor growth following US activation of 5FU-bearing MNCAs, US activation of BSA-bearing MNCAs, intravenous (i.v.) infusion of soluble 5FU, or i.v. infusion of 5FU-bearing MNCAs without US activation. *Significantly different than all other groups at same time point ($P < 0.05$). **(b)** Bar graph of fluorochrome concentration (% initial dose (ID) per gram of tissue) in tumor as a function of time following MNCA treatment at “high” and “standard” doses. **(c)** Fold change in tumor growth following US activation of 5FU-bearing MNCAs at “standard” and “high” doses, as well control groups in which 5FU-bearing MNCAs at “standard” and “high” doses were not activated with US. All values are means + SD, but many bars are not visible because they are smaller than the symbol. *Significantly different than all other groups at same time point ($P < 0.05$). **(d)** Kaplan–Meier survival curve following “high” dose 5FU-bearing MNCA treatment and i.v. soluble 5FU. *Significantly different at $P = 0.041$.

we found that delivering controlled-release NPs loaded with a drug (5FU) that is typically ineffective in this tumor model yielded positive therapeutic results. Dose-dependent tumor growth inhibition (Figures 5a,c) was observed, and animal survival improved significantly (Figure 5d). Our results broadly support the concept that covalently coupling drug-bearing, controlled-release, NPs to MBs and activating these “composite agents” with targeted US may be an effective drug delivery strategy. Such approaches could eventually serve to lower the required dosages of drugs that generate harmful side effects and/or improve the effectiveness of drugs that are difficult to concentrate in tumors.

Coinjection and composite agent strategies for NP delivery to US-targeted tumors

Drug and/or gene-bearing NPs offer advantages over many current approaches in the treatment of solid tumors; however, NP size, tumor interstitial pressure, and tumor matrix composition and charge limit NP delivery. In this study, we show that NP delivery approaches that combine US and MBs may be used to overcome these barriers when applied in the context of a solid tumor model. Applying US to tumors after the coinjection of MBs and NPs elicited a moderate, but significant, increase in NP delivery when

compared to contralateral “no US” controls. Furthermore, consistent with our previous work in ischemic skeletal muscle,¹⁴ covalently linking MBs to NPs into composite agents (*i.e.*, MNCAs) before intravenous injection yielded an even greater increase in NP delivery. The mechanism(s) of enhanced NP delivery with MNCAs is not completely understood; however, we hypothesize that linking NPs to MBs increases local NP concentration in the region of insonation, thereby leading to increased payload delivery. Other factors, such as charge and agent diameter, could also have a slight impact on NP delivery. MNCAs exhibited a greater charge than MBs alone (zeta potential of -43 versus -17 mV), which would act to decrease circulation time and hinder NP delivery. On the other hand, MNCA diameter was ~ 50 nm less than typical albumin-shelled MBs, which could have improved the passage of MNCAs through the lungs and actually increased circulation time. Nonetheless, albumin shelled MBs have a blood half-life of under 2 minutes,²⁴ while greater than 90% of all i.v. injected unbound PLGA NPs in this diameter range (*i.e.*, 120–160 μm) range are cleared from the circulation in less than 5 minutes.²⁵ Thus, we hypothesize that virtually all NP delivery for both the composite agent and coinjection approaches occurred during the actual sonication phase. This hypothesis is supported by the fact

that there was no statistically significant time-dependent increase in NP delivery within any group in the study (Figure 2). Because we used FMT to determine absolute NP concentrations in tumors, we can also make comparisons to other studies in which NPs were delivered to solid tumors. Here, the activation of MNCA with US resulted in the targeted delivery of 16% ID/g at 1 hour after treatment. In comparison to studies in which NPs were molecularly targeted to tumors, this equates to a three- to 18-fold reduction in the systemic dose required to achieve comparable intratumoral NP concentrations.^{29–31} Importantly, such increased NP delivery provides a means to reduce drug-associated toxicity and improve conventional systemic chemotherapy. Nonetheless, a remaining challenge is to reduce nonspecific NP accumulation. To reduce these off target effects, future studies will likely involve the conjugation of significantly more “stealthy” secondary nanocarriers (*i.e.*, PEGylated NPs) to the MBs and/or the further optimization of US pulsing parameters to maximize NP delivery. Another necessary refinement for future translation of the technology will be to reduce NP size variability. In turn, this will serve to normalize intraparticle release kinetics and improve reproducibility.

Local distribution and mechanisms of NP delivery to tumors with US and MBs

In this study, it is likely that NPs were delivered to tissue through at least two different modes of US-induced MB activity—sonoporation and irreversible capillary permeabilization.^{32,33} Sonoporation refers to the process by which MB oscillations reversibly open pores in cell membranes and permit the transfer of NPs to the endothelium.³⁴ Conversely, irreversible capillary permeabilization occurs when inertially cavitating MBs open pores through the capillary basement membrane,³⁵ subsequently allowing NP delivery to the interstitium by convective forces.^{16,17} The potential for an US-activated MB to generate sonoporation and/or microvessel permeabilization is dependent on US settings (*i.e.*, frequency, peak-negative pressure, and duty cycle), MB parameters (diameter, compliance, and composition), and microvessel structure (diameter, strength, and thickness). Confocal microscopy revealed that NPs were both colocalized with endothelial cells and present in the extravascular space (*i.e.*, beyond the endothelial lining) for both the MNCA+US and the MB+NP+US groups, which we contend is indicative of both endothelial sonoporation and capillary wall permeabilization. However, consistent with our observations in skeletal muscle, many of the endothelial-associated NPs in the MNCA group appeared to be significantly more concentrated. The increased concentration in the MNCA group could be explained by a combination of better endothelial delivery through enhanced sonoporation, higher local NP concentration, and/or attachment to MB shell fragments. Both diffuse and amalgamated NP delivery to the extravascular space were observed in the MNCA group (Figure 4).

Going forward, we must also consider how the limitations of NP delivery using this approach will affect which tumors may be treated. First, it is obvious that only US-accessible tumors are candidates. Tumors masked by bone (*e.g.*, the ribs) and/or air (*e.g.*, the lungs) will be difficult to treat. Second, a perfused tumor vasculature will be required because it enables the transport of MNCA into the tumor mass. Avascular tumor regions can only be treated

with this approach if they are within the effective NP delivery distance from surrounding vessels. Future studies using tumors with poorer vascularity and/or necrotic cores could be useful for establishing these critical distances. Third, although a subcutaneous glioma model served as a generalized solid tumor model in our study, the activation of MNCA with the US parameters used here (*i.e.*, 1 MHz frequency and 1.2 MPa peak-negative pressure) is not appropriate for treating the infiltrative margins of intracranial tumors via the delivery NPs across the blood-brain barrier because these US parameters will elicit inertial cavitation and petechial hemorrhage.^{36–38} Instead, infiltrative brain tumors must be treated with US parameters that generate stable cavitation. These parameters may not be sufficient to drive MNCA-delivered NP aggregates deep into tissue.

Tumor growth inhibition via the targeted delivery of 5FU-bearing NPs

In this study, the targeted delivery of 5FU bearing NPs via acoustic activation of MNCA resulted in tumor growth inhibition. In addition, studies comparing 5FU-bearing NP delivery with MNCA to intravenously administered soluble 5FU showed improved survival. We reason that these therapeutic effects were primarily achieved due to the encapsulation of 5FU in PLGA NPs, which improved the pharmacokinetic profile of the drug, and covalently linking NPs to MBs, which insured a relatively high concentration of NPs at the site of permeabilization. In support, after *i.v.* 5FU infusion at “standard” and “high” doses, no significant differences in tumor growth were observed when compared to contralateral “no US” controls. Lack of growth inhibition after treatment with soluble 5FU can likely be attributed to the low initial dose (*i.e.*, 90- and 9,000-fold lower than recommend systemic dose)³⁹ and short blood half-life (11.4 minutes).⁴⁰ Similarly, treatment with US and “blank” BSA-Bearing MNCA resulted in no significant differences in tumor doubling time when compared to contralateral “no US” controls. Taken together, neither ultrasonic destruction of unloaded NPs bound to MBs nor intravenous chemotherapy was sufficient on its own to achieve the improved benefit observed when the two treatments were combined.

In addition, we must also consider that US may have potentiated local 5FU activity within the tumor due to tumor heating and/or enhanced tumor tissue permeability, which could elicit better 5FU diffusion. Indeed, it has been reported that US alone may increase the antitumor activity of 5FU,⁴¹ and the acoustic activation of MBs in combination with 5FU has been reported to be more effective than 5FU alone or in combination with US.⁴² Bulk tumor heating was unlikely with this particular protocol, as previously demonstrated by our group.²⁶ Nonetheless, while bulk intratumor temperature likely did not increase significantly during treatment, MB cavitation is known to induce focal “hot spots.”⁴³ Regional hyperthermia in addition to chemotherapy has been demonstrated to be more effective than chemotherapy in certain applications.⁴⁴

We also report that treatment with “high” dose 5FU-MNCA elicited statistically significant reductions in tumor volume when compared to treatment with “standard” dose 5FU-MNCA. While these results are generally consistent with studies demonstrating dose-dependent tumor growth inhibition in response

to 5FU treatment,^{45,46} we expected to observe more robust tumor growth inhibition in response to the ~100-fold increase in local 5FU NP delivery (estimated by considering the 100-fold increase in administered MNCA dosage along with the NP delivery data). There are, however, some potential explanations. First, 5FU directed DNA and RNA damage occur in S and G1 phases, respectively;⁴⁷ therefore, cells in S and G1 are preferentially affected. The controlled release of 5FU from NPs prolongs the exposure of tumor cells to the drug; however, 5FU was not released as a zero-order function. Therefore, the advantage conferred by using controlled-release NPs may have diminished with time, with cells entering S and/or G1 phase a few days after treatment being exposed to less drug. Furthermore, it has been shown that drug release from the NPs may have been affected by US and US+MB interactions,⁴⁸ so the release curve may have been further modified *in vivo*. Thus, improvements in the kinetics of drug release from the NPs via fine-tuning of polymer composition and/or drug loading could improve treatment. Second, even in the face of higher 5FU concentrations and improved local delivery kinetics, drug resistance due to increased 5FU efflux, increased tolerance to DNA damage, deregulation of pyrimidine metabolism related enzymes, and/or the overexpression of antiapoptotic factors may have allowed a population of cancer cells to progress. Third, it is likely that NPs were not uniformly distributed within the tumor following MNCA+US treatment. The extent of MNCA+US mediated NP delivery within a tumor region is dependent on local MNCA concentration, which in turn depends on perfusion. Tumor perfusion is heterogeneous and generally lower in the tumor core,⁴⁹ so poorly perfused tumor regions may have still been undertreated in the “high” dose group. Going forward, treatment limitations associated with poor local tumor perfusion could be addressed by “normalizing” the tumor microvasculature, leading to more uniform perfusion, and/or improving intratumor NP diffusion via the addition of a PEG coating to neutralize zeta-potential. Of course, such a modification would also improve circulation time, leading to enhanced delivery overall.

MATERIALS AND METHODS

Tumor model. All animal procedures were conducted with the approval of the Institutional Animal Care and Use Committee, and all procedures were followed in accordance with institutional guidelines. The C6 Glioma rat tumor cell line was maintained in F-12K Nutrient Mixture (Gibco, Carlsbad, CA) supplemented with 16% horse serum (Sigma, St Louis, MO), 3% fetal bovine serum (Sigma), and 1% pen-strep (Gibco) at 37 °C and 5% CO₂. Tumors were generated *in vivo* by injecting 3 × 10⁶ tumor cells suspended in 300 μl of phosphate-buffered saline subcutaneously into the right and/or left hindlimbs of C57BL/6J-Rag-1 mice ranging from 20 to 25 g in body weight. Tumors were allowed to grow for 7–12 days, reaching a diameter of 8–10 mm before treatment.

MB fabrication. To prepare albumin MBs, a 1% solution of serum albumin in normal saline was placed in a flask with a blanket atmosphere of octafluoropropane gas above the aqueous phase. The solution was briefly sonicated (29 kHz, 30 seconds) with an US disintegrator (XI2020; Misonix, Farmingdale, NY) equipped with an extended ½” titanium probe. Large MBs were separated by flotation in a vertically positioned 3 ml syringe and discarded. After purification, the remaining MBs were placed in glass vials, stoppered and sealed under octafluoropropane atmosphere.

NP and MB-NP composite agent fabrication, characterization, and delivery. Procedures for NP fabrication, conjugation of VivoTag 680 to NPs, MNCA fabrication, cytometry imaging, 5FU loading, and tissue processing are provided in the **Supplementary Materials and Methods** section.

NP delivery to tumors by ultrasonic MB destruction. On the day of treatment, animals were anesthetized with an intraperitoneal combination injection of ketamine hydrochloride (1.56 ml/kg body weight), xylazine (0.52 ml/kg body weight), and sterilized water (3.12 ml/kg body weight). In bilateral tumor NP delivery evaluation studies, the tail vein was cannulated for i.v. administration of either a coinjection of MBs and NPs ($n = 4$ mice; 1 × 10⁵ MBs/g and 0.2 μg NPs/g body weight in 0.30 ml of 0.9% saline), MNCAs ($n = 4$ mice; 1 × 10⁵ MNCAs/g body weight in 0.3 ml of 0.9% saline) or NPs ($n = 4$ mice; 0.2 μg NPs/g body weight in 0.30 ml of 0.9% saline). In bilateral tumor therapeutic efficacy studies, the tail vein of each animal was cannulated for i.v. administration of either 5FU-bearing MNCAs at a “standard” ($n = 6$ mice; 1 × 10⁵ MNCAs/g body weight in 0.3 ml of 0.9% saline) or “high” ($n = 4$ mice; 1 × 10⁷ MNCAs/g body weight in 0.3 ml of 0.9% saline) dose, BSA-bearing MNCAs ($n = 4$; 1 × 10⁵ MNCAs/g body weight in 0.3 ml of 0.9% saline), or a soluble 5FU ($n = 4$; 30 ng) solution concentration matched to the “standard” 5FU-MNCA dose. In unilateral tumor survival studies, the tail vein was cannulated for i.v. administration of either 5FU-MNCAs at a “high” dose ($n = 6$ mice; 1 × 10⁷ MNCAs/g body weight in 0.3 ml of 0.9% saline) or a soluble 5FU ($n = 6$; 3 μg) solution with a concentration matched to the “high” 5FU-MNCA dose. Tail vein catheters consisted of a 27½ gauge needle connected to 12 inches of PE20 polyethylene tubing (BPE-T20, PE-20 tubing, 0.015”ID × 0.043”OD). Heparinized saline (0.9%) was used to clear the 200 μl of catheter dead space.

A water-based US gel (Aquasonic 100; Parker Laboratories, Fairfield, NJ) was applied to the skin above the flank tumor, and a 0.75” diameter 1 MHz unfocused transducer (A314S; Panametrics, Waltham, MA) was coupled to the skin. Injection duration (68 minutes) and rate (5 μl/minute) were controlled by an infusion pump (Harvard Apparatus PHD 2000; Harvard Apparatus, Holliston, MA). The dead space of the tail vein catheter was cleared prior to initiating US pulsing. Each pulse consisted of 100 consecutive 1 MHz sinusoids of 1V peak-to-peak amplitude applied every 5 seconds for 60 minutes. Sinusoids were each of 1V peak to peak amplitude from a waveform generator (AFG-310; Tektronix, Beaverton, OR). The waveform signal was amplified by a 55 dB RF power amplifier (ENI 3100LA; Electronic Navigation Industries, Richardson, TX). Maximum peak negative pressure, as measured with a needle hydrophone (Specialty Engineering Associates, Sunnyvale, CA; Model PVDF-Z44-0400) was 1.2 MPa. Pulsing parameters were chosen based on previous studies from our group wherein NPs were delivered to relatively large tissue volumes using unfocused transducers.^{19,20,22}

Tumor growth rate. The volumes (V) of tumors treated with BSA-MNCAs ± US, 5FU-MNCAs ± US and soluble 5FU were evaluated by taking daily measurements with digital calipers. Volume was calculated using an ellipsoid approximation; $V = 1/6 \pi abc$. Where a, b, and c are the maximum diameters of the tumor measured in three orthogonal planes. Fold increase in tumor volume was defined as the tumor volume at “x” days following treatment divided by the tumor volume prior to treatment.

Survival analysis. Population curves were plotted using the Kaplan–Meier method, where the maximum tumor volume was 1400 mm.³

Statistical analysis. Data in **Figures 2b** and **5a–c** were analyzed by two-way repeated measures analysis of variance followed by pairwise comparisons with the Holm–Sidak method. Significance was assessed at $P < 0.05$. Survival data in **Figure 5d** were analyzed by a Wilcoxon rank-sum test. Significance was assessed at $P < 0.05$. All statistical analyses were undertaken using SigmaStat 3.5 (Systat Software, San Jose, Ca).

SUPPLEMENTARY MATERIAL

Materials and Methods

ACKNOWLEDGMENTS

This study was supported by grants from The Hartwell Foundation, the Focused Ultrasound Surgery Foundation, and the National Institutes of Health (R01 CA164789).

REFERENCES

- Chen, Y, Jungsuwadee, P, Vore, M, Butterfield, DA and St Clair, DK (2007). Collateral damage in cancer chemotherapy: oxidative stress in nontargeted tissues. *Mol Interv* **7**: 147–156.
- Boucher, Y, Baxter, LT and Jain, RK (1990). Interstitial pressure gradients in tissue-isolated and subcutaneous tumors: implications for therapy. *Cancer Res* **50**: 4478–4484.
- Jain, RK (1988). Transvascular and interstitial transport in tumors. *Adv Exp Med Biol* **242**: 215–220.
- Jain, RK (1990). Vascular and interstitial barriers to delivery of therapeutic agents in tumors. *Cancer Metastasis Rev* **9**: 253–266.
- Stylianopoulos, T, Poh, MZ, Insin, N, Bawendi, MG, Fukumura, D, Munn, LL et al. (2010). Diffusion of particles in the extracellular matrix: the effect of repulsive electrostatic interactions. *Biophys J* **99**: 1342–1349.
- Chan, JM, Valencia, PM, Zhang, L, Langer, R and Farokhzad, OC (2010). Polymeric nanoparticles for drug delivery. *Methods Mol Biol* **624**: 163–175.
- Matsumura, Y and Maeda, H (1986). A new concept for macromolecular therapeutics in cancer chemotherapy: mechanism of tumorotropic accumulation of proteins and the antitumor agent smancs. *Cancer Res* **46**(12 Pt 1): 6387–6392.
- Tréhin, R, Figueiredo, JL, Pittet, MJ, Weissleder, R, Josephson, L and Mahmood, U (2006). Fluorescent nanoparticle uptake for brain tumor visualization. *Neoplasia* **8**: 302–311.
- Perrault, SD, Walkey, C, Jennings, T, Fischer, HC and Chan, WC (2009). Mediating tumor targeting efficiency of nanoparticles through design. *Nano Lett* **9**: 1909–1915.
- Skyba, DM, Price, RJ, Linka, AZ, Skalak, TC and Kaul, S (1998). Direct *in vivo* visualization of intravascular destruction of microbubbles by ultrasound and its local effects on tissue. *Circulation* **98**: 290–293.
- Ward, M, Wu, J and Chiu, JF (1999). Ultrasound-induced cell lysis and sonoporation enhanced by contrast agents. *J Acoust Soc Am* **105**: 2951–2957.
- Ferrara, K, Pollard, R and Borden, M (2007). Ultrasound microbubble contrast agents: fundamentals and application to gene and drug delivery. *Annu Rev Biomed Eng* **9**: 415–447.
- Ferrara, KW, Borden, MA and Zhang, H (2009). Lipid-shelled vehicles: engineering for ultrasound molecular imaging and drug delivery. *Acc Chem Res* **42**: 881–892.
- Burke, CW, Hsiang, YH, Alexander, E 4th, Kilbanov, AL and Price, RJ (2011). Covalently linking poly(lactic-co-glycolic acid) nanoparticles to microbubbles before intravenous injection improves their ultrasound-targeted delivery to skeletal muscle. *Small* **7**: 1227–1235.
- Chappell, JC, Song, J, Burke, CW, Kilbanov, AL and Price, RJ (2008). Targeted delivery of nanoparticles bearing fibroblast growth factor-2 by ultrasonic microbubble destruction for therapeutic arteriogenesis. *Small* **4**: 1769–1777.
- Price, RJ, Skyba, DM, Kaul, S and Skalak, TC (1998). Delivery of colloidal particles and red blood cells to tissue through microvessel ruptures created by targeted microbubble destruction with ultrasound. *Circulation* **98**: 1264–1267.
- Song, J, Chappell, JC, Qi, M, VanGieson, EJ, Kaul, S and Price, RJ (2002). Influence of injection site, microvascular pressure and ultrasound variables on microbubble-mediated delivery of microspheres to muscle. *J Am Coll Cardiol* **39**: 726–731.
- Vancraeynest, D, Havaux, X, Pouleur, AC, Pasquet, A, Gerber, B, Beauloye, C et al. (2006). Myocardial delivery of colloid nanoparticles using ultrasound-targeted microbubble destruction. *Eur Heart J* **27**: 237–245.
- Rapoport, N, Gao, Z and Kennedy, A (2007). Multifunctional nanoparticles for combining ultrasonic tumor imaging and targeted chemotherapy. *J Natl Cancer Inst* **99**: 1095–1106.
- Kheirloom, A, Dayton, PA, Lum, AF, Little, E, Paoli, EE, Zheng, H et al. (2007). Acoustically-active microbubbles conjugated to liposomes: characterization of a proposed drug delivery vehicle. *J Control Release* **118**: 275–284.
- Lum, AF, Borden, MA, Dayton, PA, Kruse, DE, Simon, SI and Ferrara, KW (2006). Ultrasound radiation force enables targeted deposition of model drug carriers loaded on microbubbles. *J Control Release* **111**: 128–134.
- Lentacker, I, Wang, N, Vandenbroucke, RE, Demeester, J, De Smedt, SC and Sanders, NN (2009). Ultrasound exposure of lipoplex loaded microbubbles facilitates direct cytoplasmic entry of the lipoplexes. *Mol Pharm* **6**: 457–467.
- Vandenbroucke, RE, Lentacker, I, Demeester, J, De Smedt, SC and Sanders, NN (2008). Ultrasound assisted siRNA delivery using PEG-siPlex loaded microbubbles. *J Control Release* **126**: 265–273.
- Hutter, JC, Luu, HM-D, Mehlhaff, PM, Killam, AL and Dittrich, HC (1999). Physiologically based pharmacokinetic model for fluorocarbon elimination after the administration of an octafluoropropane-albumin microsphere sonographic contrast agent. *J Ultrasound Med* **18**: 1–11.
- Gref, R, Minamitake, Y, Peracchia, MT, Trubetskoy, V, Torchilin, V and Langer, R (1994). Biodegradable long-circulating polymeric nanospheres. *Science* **263**: 1600–1603.
- Burke, CW, Kilbanov, AL, Sheehan, JP and Price, RJ (2011). Inhibition of glioma growth by microbubble activation in a subcutaneous model using low duty cycle ultrasound without significant heating. *J Neurosurg* **114**: 1654–1661.
- Chumakova, OV, Liopo, AV, Andreev, VG, Cicenaitis, I, Evers, BM, Chakrabarty, S et al. (2008). Composition of PLGA and PEI/DNA nanoparticles improves ultrasound-mediated gene delivery in solid tumors *in vivo*. *Cancer Lett* **261**: 215–225.
- Kaplan, EL and Meier P (1958). Nonparametric estimation from incomplete observations. *J Am Stat Assoc* **53**: 457–481.
- Cai, W, Chen, K, Li, ZB, Gambhir, SS and Chen, X (2007). Dual-function probe for PET and near-infrared fluorescence imaging of tumor vasculature. *J Nucl Med* **48**: 1862–1870.
- Natarajan, A, Gruettner, C, Ivkov, R, DeNardo, GL, Mirick, G, Yuan, A et al. (2008). NanoFerrite particle based radioimmunonanoparticles: binding affinity and *in vivo* pharmacokinetics. *Bioconjug Chem* **19**: 1211–1218.
- Melancon, MP, Lu, W, Yang, Z, Zhang, R, Cheng, Z, Elliot, AM et al. (2008). *In vitro* and *in vivo* targeting of hollow gold nanoshells directed at epidermal growth factor receptor for photothermal ablation therapy. *Mol Cancer Ther* **7**: 1730–1739.
- Meijering, BD, Juffermans, LJ, van Wamel, A, Henning, RH, Zuhorn, IS, Emmer, M et al. (2009). Ultrasound and microbubble-targeted delivery of macromolecules is regulated by induction of endocytosis and pore formation. *Circ Res* **104**: 679–687.
- van Wamel, A, Kooiman, K, Emmer, M, ten Cate, FJ, Versluis, M and de Jong, N (2006). Ultrasound microbubble induced endothelial cell permeability. *J Control Release* **116**: e100–e102.
- Liang, HD, Tang, J and Halliwell, M (2010). Sonoporation, drug delivery, and gene therapy. *Proc Inst Mech Eng H* **224**: 343–361.
- Qin, S and Ferrara, KW (2006). Acoustic response of compliant microvessels containing ultrasound contrast agents. *Phys Med Biol* **51**: S065–S088.
- Konofagou, EE (2012). Optimization of the ultrasound-induced blood-brain barrier opening. *Theranostics* **2**: 1223–1237.
- Tung, YS, Vlachos, F, Feshitan, JA, Borden, MA and Konofagou, EE (2011). The mechanism of interaction between focused ultrasound and microbubbles in blood-brain barrier opening in mice. *J Acoust Soc Am* **130**: 3059–3067.
- Arvanitis, CD, Livingstone, MS, Vykhodtseva, N and McDannold, N (2012). Controlled ultrasound-induced blood-brain barrier disruption using passive acoustic emissions monitoring. *PLoS ONE* **7**: e45783.
- Blumenthal, RD, Osorio, L, Ochakovskaya, R, Ying, Z and Goldenberg, DM (2000). Regulation of tumour drug delivery by blood flow chronobiology. *Eur J Cancer* **36**: 1876–1884.
- MacMillan, WE, Wolberg, WH and Welling, PG (1978). Pharmacokinetics of fluorouracil in humans. *Cancer Res* **38**: 3479–3482.
- Mohamed, MM, Mohamed, MA and Fikry, NM (2003). Enhancement of antitumor effects of 5-fluorouracil combined with ultrasound on Ehrlich ascites tumor *in vivo*. *Ultrasound Med Biol* **29**: 1635–1643.
- Chumakova, OV, Liopo, AV, Evers, BM and Esenaliev, RO (2006). Effect of 5-fluorouracil, Optison and ultrasound on MCF-7 cell viability. *Ultrasound Med Biol* **32**: 751–758.
- Klotz, AR, Lindvere, L, Stefanovic, B and Hynynen, K (2010). Temperature change near microbubbles within a capillary network during focused ultrasound. *Phys Med Biol* **55**: 1549–1561.
- Issels, RD, Lindner, LH, Verweij, J, Wust, P, Reichardt, P, Schem, BC et al.; European Organisation for Research and Treatment of Cancer Soft Tissue and Bone Sarcoma Group (EORTC-STBSG); European Society for Hyperthermic Oncology (ESHO). (2010). Neo-adjuvant chemotherapy alone or with regional hyperthermia for localised high-risk soft-tissue sarcoma: a randomised phase 3 multicentre study. *Lancet Oncol* **11**: 561–570.
- Senderoff, RJ, Weber, PA, Smith, DR and Sokoloski, TD (1990). Evaluation of antiproliferative agents using a cell-culture model. *Invest Ophthalmol Vis Sci* **31**: 2572–2578.
- Hasegawa, Y, Goto, M, Hanai, N, Ijichi, K, Adachi, M, Terada, A et al. (2007). Evaluation of optimal drug concentration in histoculture drug response assay in association with clinical efficacy for head and neck cancer. *Oral Oncol* **43**: 749–756.
- Mirjolet, JF, Didelot, C, Barberi-Heyob, M and Merlin, JL (2002). G(1)/S but not G(0)/G(1) cell fraction is related to 5-fluorouracil cytotoxicity. *Cytometry* **48**: 6–13.
- Agrawal, CM, Kennedy, ME and Micallef, DM (1994). The effects of ultrasound irradiation on a biodegradable 50-50% copolymer of polylactic and polyglycolic acids. *J Biomed Mater Res* **28**: 851–859.
- Silva, AC, Kim, SG and Garwood, M (2000). Imaging blood flow in brain tumors using arterial spin labeling. *Magn Reson Med* **44**: 169–173.